Обзор ArXiv/astro-ph, 15-22 сентября 2025

От Сильченко О.К.

ArXiv:2509.15405

Caught in the Cosmic Web: Evidence for Ram-Pressure Stripping of a Low-Mass Galaxy by the Cosmic Web

Nicholas Luber, ¹ Sabrina Stierwalt, ² George C. Privon, ^{3,4,5} Gurtina Besla, ⁶ Kelsey E. Johnson, ⁴ Nitya Kallivayalil, ⁴ David R. Patton, ⁷ Mary Putman, ¹ and Jingyao Zhu¹

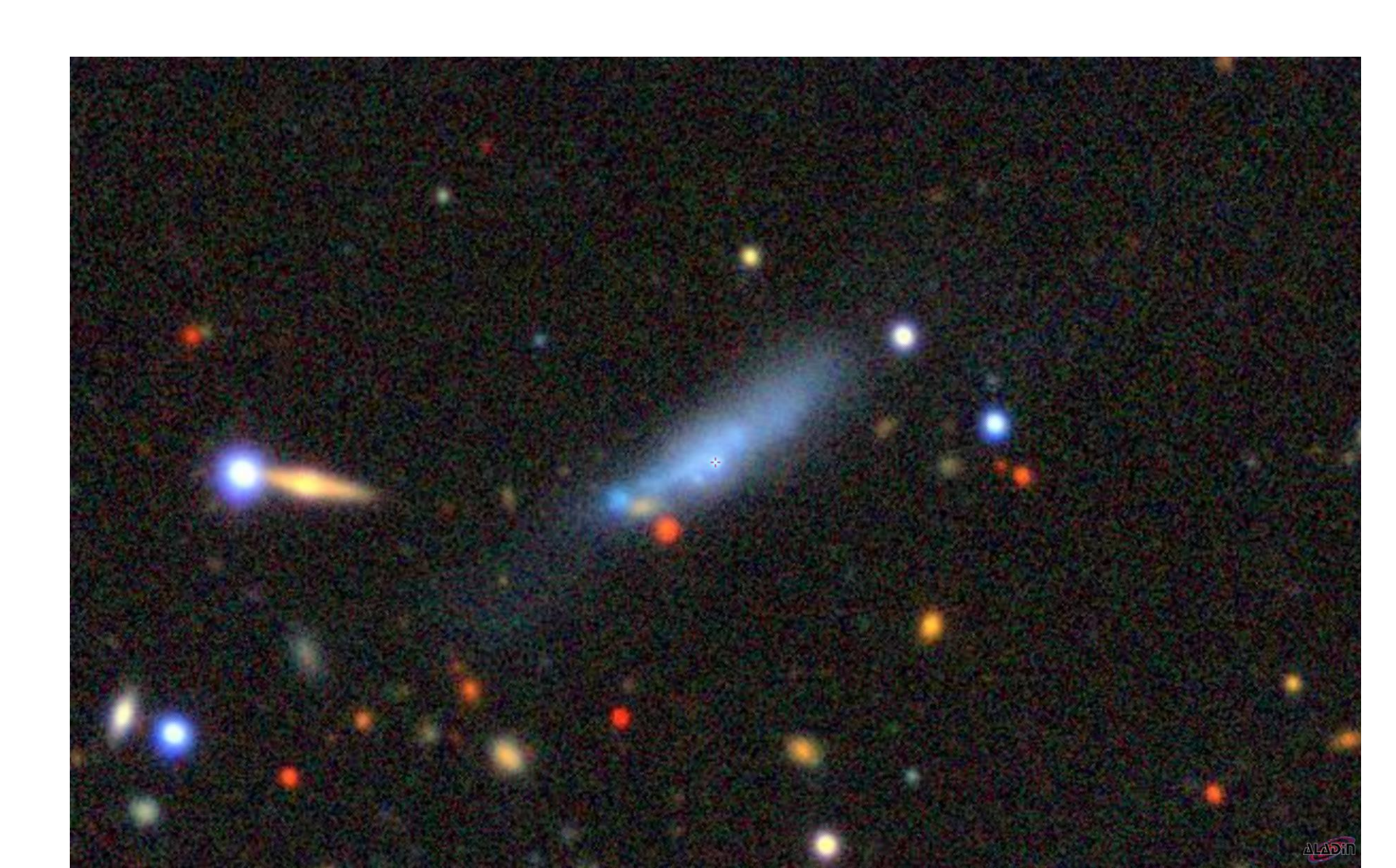
¹Department of Astronomy, Columbia University, Mail Code 5247, 538 West 120th Street, New York, NY 10027, USA
 ²Department of Physics, Occidental College, 1600 Campus Road, Los Angeles, CA 90041, USA
 ³National Radio Astronomy Observatory, 520 Edgemont Road, Charlottesville, VA 22903, USA
 ⁴Department of Astronomy, University of Virginia, 530 McCormick Road, Charlottesville, VA 22904 USA
 ⁵Department of Astronomy, University of Florida, P.O. Box 112055, Gainesville, FL 32611, USA
 ⁶Department of Astronomy, University of Arizona, 933 North Cherry Avenue, Tucson, AZ 85721
 ⁷Department of Physics & Astronomy, Trent University, 1600 West Bank Drive, Peterborough, Ontario, Canada K9L OG2

(Received 26 August 2025; Revised 12 September 2025; Accepted 18 September 2025)

ABSTRACT

We present interferometric radio observations of the neutral atomic gas in AGC 727130, a low-mass, gas-rich, field galaxy lacking significant star-formation. The atomic gas in AGC 727130 displays a pronounced asymmetry, extending well beyond the stellar disk in one direction while remaining relatively undisturbed in the other. Despite proximity to a pair of interacting dwarfs, tidal analysis suggests these neighboring galaxies are not responsible for this pronounced asymmetry. Instead, using a topological cosmic web filament finder on spectroscopic catalogue data, we find AGC 727130 lies at the intersection of several large-scale cosmic web filaments, environments predicted to host diffuse, shock-heated gas. We propose that an interaction with this ambient medium is stripping gas from the galaxy via cosmic web ram-pressure stripping. This mechanism, supported by recent simulations, may quench low-mass galaxies outside of massive halos, and must be accounted for when comparing observed numbers of dwarf galaxies to theoretical predictions.

AGC 727130, DECaLS



Свойства карликовой галактики

- Открыта в обзоре ALFALFA, V_r=~2000
- Далее картирование в 21 см VLA с разрешением 7.5"
- Macca HI 3.5 10⁸
- Звездная масса 7 10⁷
- Никакой H-alpha
- No radiocontinuum 1.4 ГГц
- Верхний предел на SFR 1.2 10⁻³

HI

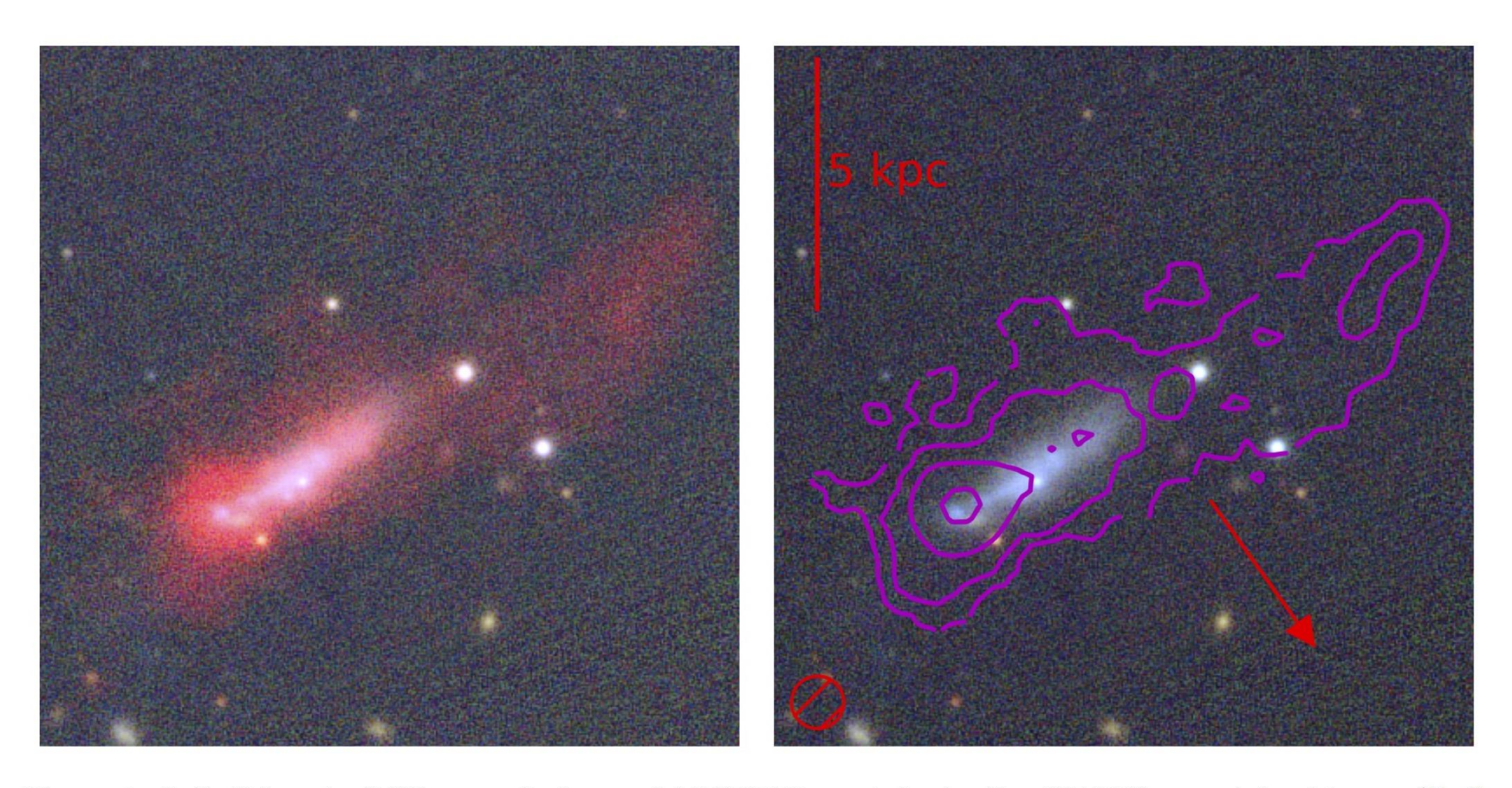


Figure 1. Left: False-color RGB composite image of AGC727130, created using Pan-STARRS g-, r-, i- band images (K. C. Chambers et al. 2016), with a red-scale overlay showing the spatial distribution of the neutral atomic gas. This image is oriented with north pointing upwards, and west pointing rightwards. Right: The same optical image, with HI column density contours overlaid with levels $2^n \times 10^{20}$ atoms cm⁻² for n = 1, 2, 3, 4. The hatched circle in the bottom left corresponds to the restoring beam for the HI observations, the red scale bar in the top left corresponds to 5 kpc in projection, and the arrow in the bottom right points to the direction of the interacting pair 60 kpc away in projection.

PV-diagram along major axis

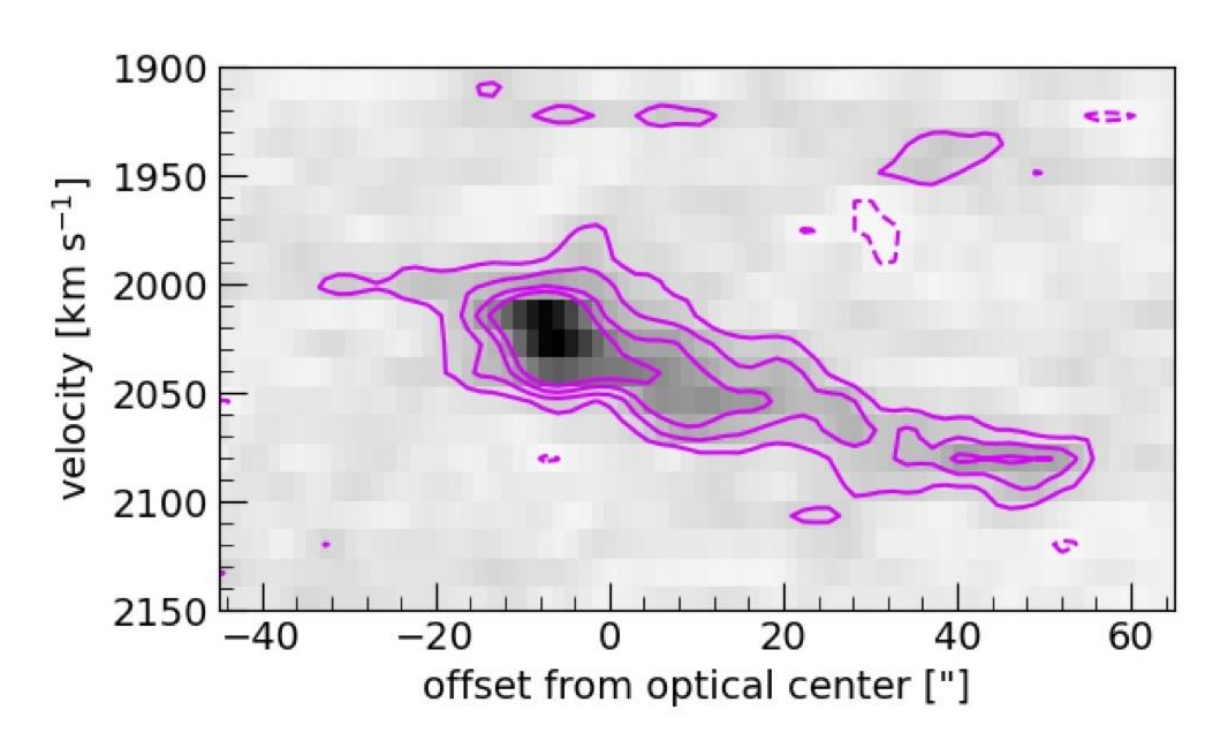


Figure 2. A position-velocity diagram taken across the major axis of the galaxy. The x-axis corresponds to the angular offset along the axis from optical center, the y-axis velocity corresponds to the observed line-of-sight velocity, and the greyscale and contours indicate the intensity level.

Положение относительно филаментов: ram-pressure?

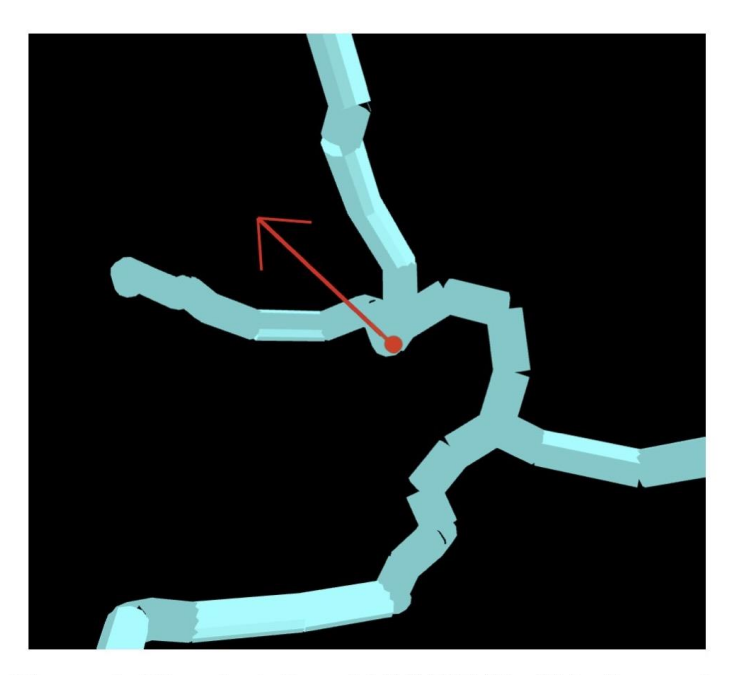


Figure 3. The orientation of AGC 727130 within the cosmic web. The blue cylinders indicate the spine of the filamentary network, as outputted by DisPerSE, and their width corresponds to 1 Mpc. The red dot marks the position of AGC 727130, and we note that the galaxy is placed within the intersection of the filaments at this point. The arrow indicates the direction of the asymmetric HI extension, corresponding to pointing towards the northwest in the plane-of-the-sky as seen in Figure 1.

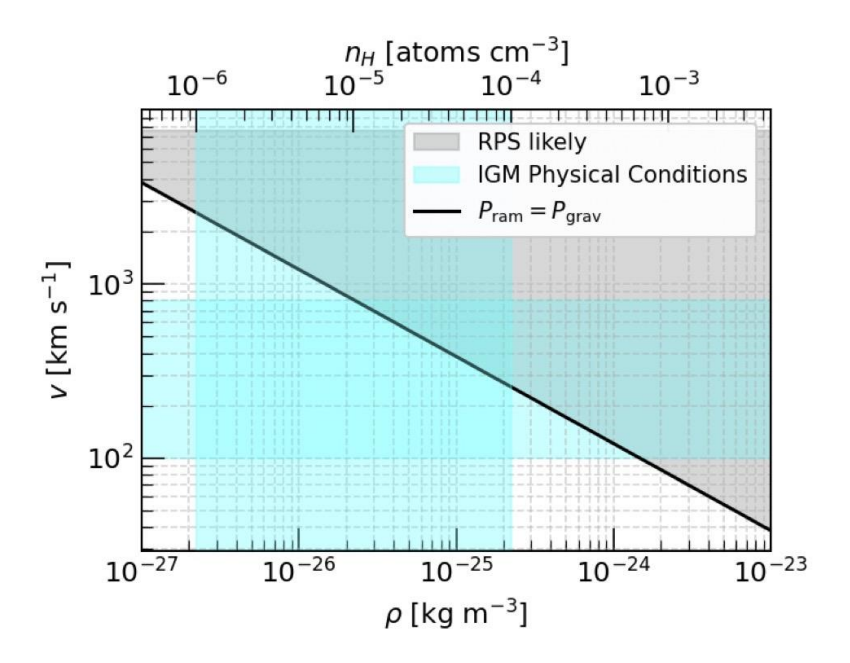


Figure 4. Ram pressure stripping criterion for AGC 727130. The grey-shaded region indicates combinations of intergalactic medium density and galaxy velocity where the external ram pressure exceeds the galaxy's restoring force, making gas removal via ram-pressure stripping likely. The cyan regions correspond to the regions of parameter space expected in cosmic web filaments.

ArXiv: 2509.12316

Building up JWST-SUSPENSE: inside-out quenching at cosmic noon from age, Fe-, and Mg-abundance gradients

Chloe M. Cheng^{1,*}, Martje Slob¹, Mariska Kriek¹, Aliza G. Beverage², Guillermo Barro³, Rachel Bezanson⁴, Anna de Graaff⁵, Natascha M. Förster Schreiber⁶, Brian Lorenz², Danilo Marchesini⁷, Ignacio Martín-Navarro^{8,9}, Adam Muzzin¹⁰, Andrew B. Newman¹¹, Sedona H. Price¹², Katherine A. Suess¹³, Arjen van der Wel¹⁴, Jesse van de Sande¹⁵, Pieter G. van Dokkum¹⁶, and Daniel R. Weisz²

- ¹ Leiden Observatory, Leiden University, P.O. Box 9513, 2300 RA Leiden, The Netherlands
- ² Department of Astronomy, University of California, Berkeley, CA 94720, USA
- ³ University of the Pacific, Stockton, CA 90340 USA
- ⁴ Department of Physics & Astronomy and PITT PACC, University of Pittsburgh, Pittsburgh, PA 15260, USA
- ⁵ Max-Planck-Institut für Astronomie, Königstuhl 17, D-69117, Heidelberg, Germany
- ⁶ Max-Planck-Institut für extraterrestrische Physik, Giessenbachstrasse 1, D-85748 Garching, Germany
- ⁷ Department of Physics & Astronomy, Tufts University, MA 02155, USA
- ⁸ Instituto de Astrofísica de Canarias,c/ Vía Láctea s/n, E38205 La Laguna, Tenerife, Spain
- ⁹ Departamento de Astrofísica, Universidad de La Laguna, E-38205 La Laguna, Tenerife, Spain
- Department of Physics and Astronomy, York University, 4700 Keele Street, Toronto, Ontario, ON MJ3 1P3, Canada
- Observatories of the Carnegie Institution for Science, 813 Santa Barbara Street, Pasadena, CA 91101, USA
- ¹² Space Telescope Science Institute (STScI), 3700 San Martin Drive, Baltimore, MD 21218, USA
- ¹³ Department for Astrophysical & Planetary Science, University of Colorado, Boulder, CO 80309, USA
- ¹⁴ Sterrenkundig Observatorium, Universiteit Ghent, Krijgslaan 281 S9, B-9000 Gent, Belgium
- ¹⁵ School of Physics, University of New South Wales, Sydney, NSW 2052, Australia
- ¹⁶ Astronomy Department, Yale University, 52 Hillhouse Avenue, New Haven, CT 06511, USA

Выборка

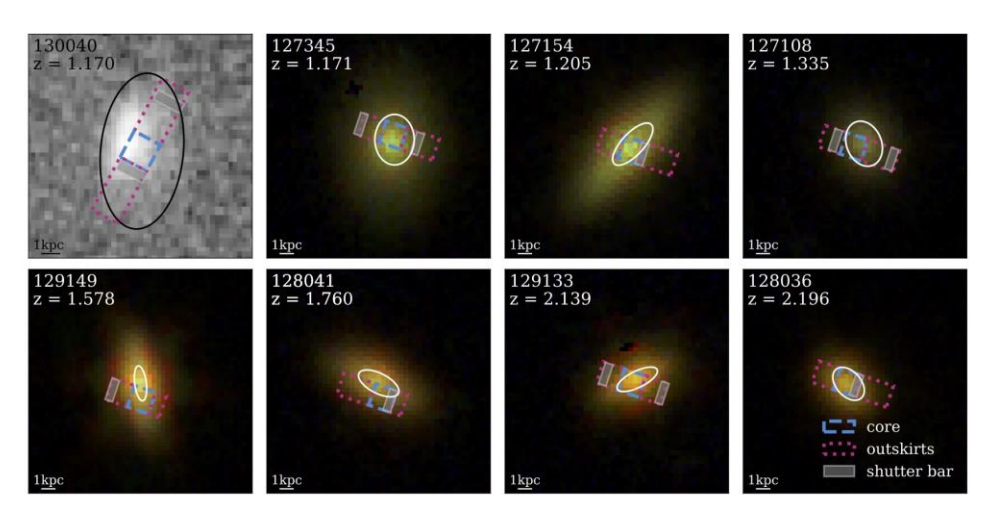


Fig. 1. Colour image cutouts of the 8 distant, quiescent galaxies in our sample. Seven galaxies have NIRCam imaging, which we combine into RGB images here. Galaxy 130040 does not have NIRCam imaging, so we show a cutout of the COSMOS HST/ACS F814W image (Koekemoer et al. 2007; Scoville et al. 2007, note that this image is rotated by 90 degrees compared to the NIRCam images). We highlight the regions that we combine for the core and outskirt spectra in blue and pink, respectively (see Section 3.2). We also indicate where shutter bars lie within these core and outskirt regions with shaded rectangles. We indicate $1 R_e$ in convolved space for each galaxy with an ellipse (see Section 3.3).

Table 1. Our sample of massive quiescent galaxies from *JWST*-SUSPENSE.

		$\log(M_*)^a$	Kinematic		
ID	$z_{\rm spec}^{\ a}$		V_{r_c}/σ_0 σ_0		$R_{\rm e}^{ m b}$
		$({ m M}_{\odot})$		(km/s)	(arcsecond)
130040	1.170	11.1	$0.63^{+0.06}_{-0.07}$	285+5	0.62°
127345	1.171	10.7	-	- "	0.18 ± 0.08
127154	1.205	10.8	-	242^{+4}_{-6}	0.25 ± 0.05
127108	1.335	10.3	$0.54^{+0.12}_{-0.20}$	210^{+5}_{-10}	0.17 ± 0.08
129149	1.578	11.0	$0.49^{+0.07}_{-0.12}$	387^{+4}_{-34}	0.12 ± 0.01
128041	1.760	10.7	$1.48^{+0.07}_{-0.06}$	226_{-1}^{+1}	0.19 ± 0.05
129133	2.139	11.1	$1.19^{+0.07}_{-0.07}$	257^{+2}_{-1}	0.19 ± 0.10
128036	2.196	11.0	$1.18^{+0.09}_{-0.08}$	210_{-6}^{+3}	0.13 ± 0.03

^a Presented in Slob et al. (2024).
^b Presented in Slob et al. (2025).

^c Presented in Griffith et al. (2012).

Суммарный спектр

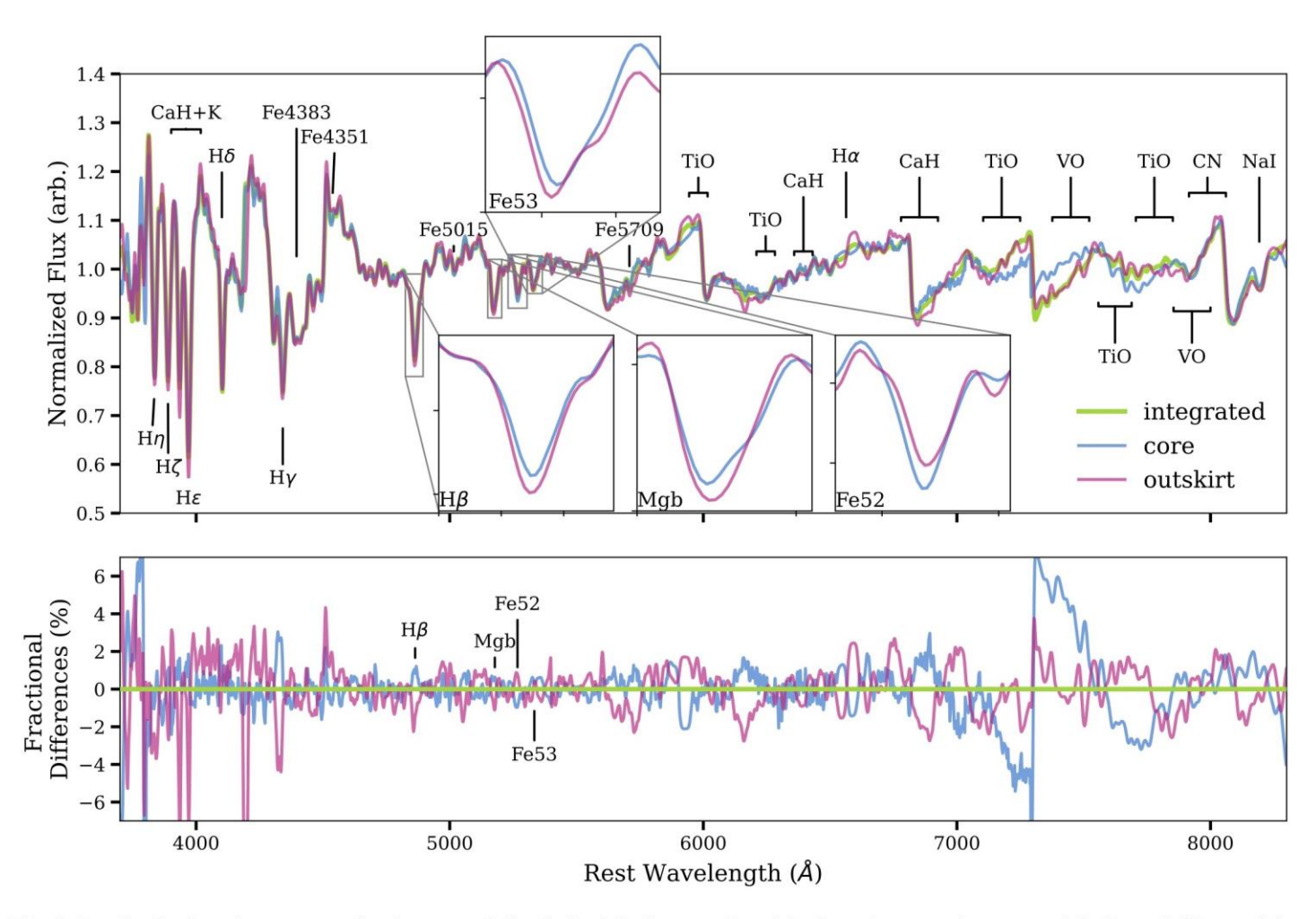


Fig. 2. Top: Stack of continuum-normalized spectra of all galaxies. The integrated stack is shown in green, the core stack is shown in blue, and the outskirt stack is shown in magenta. We label key spectral features. In the inset panels, we zoom-in on the $H\beta$ ($\sim 4849 - 4878$ Å, sensitive to age), Mgb ($\sim 5162 - 5194$ Å, sensitive to [Mg/H]), Fe52 ($\sim 5247 - 5287$ Å, sensitive to age and [Fe/H]), and Fe53 ($\sim 5314 - 5454$ Å, sensitive to age and [Fe/H]) features in the core and outskirt spectra. Bottom: The fractional differences of each stacked spectrum, where we divide each spectrum by the stacked integrated spectrum.

Индивидуальные спектры

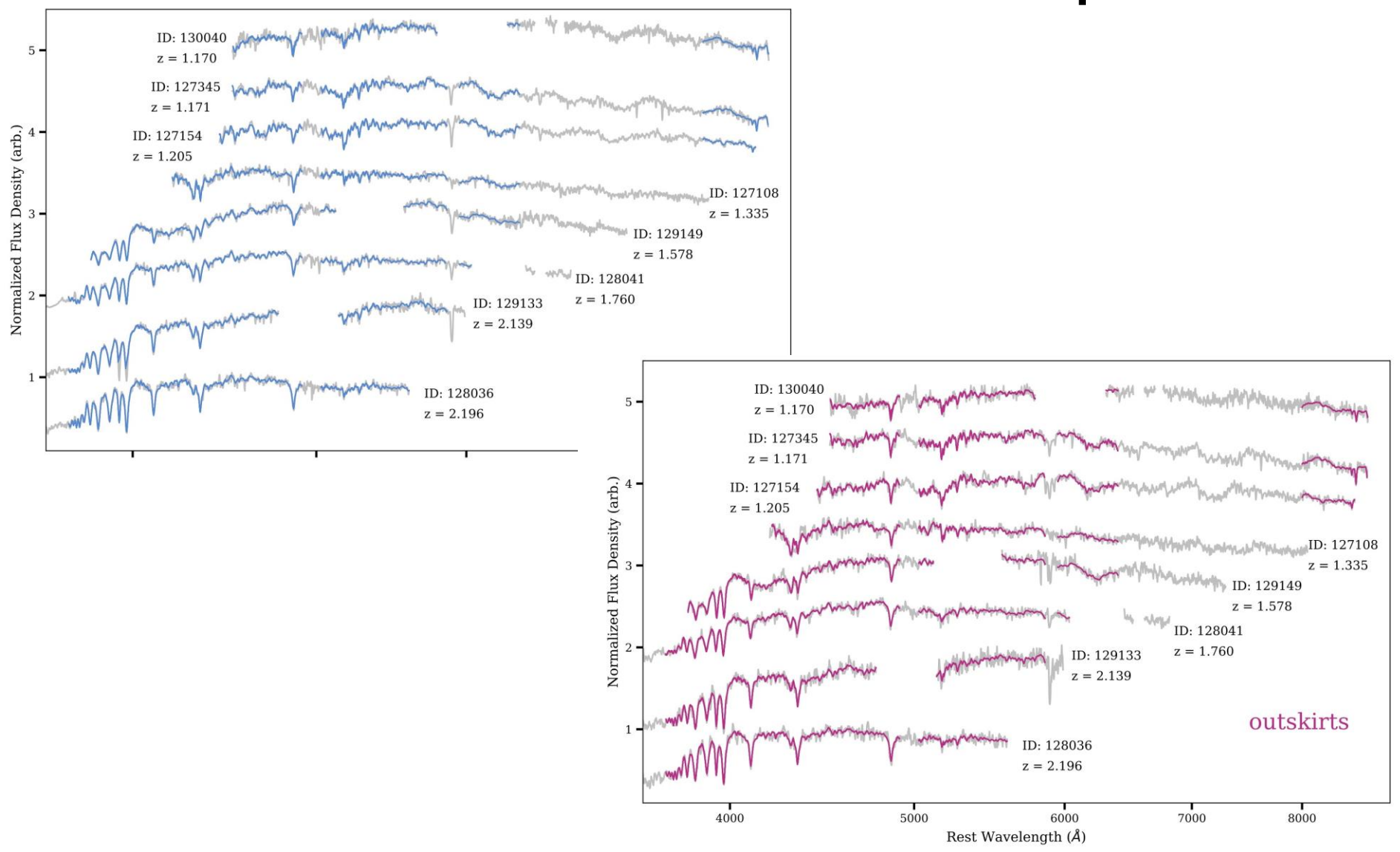


Fig. 3. Best-fitting ALF α models to our quiescent galaxy spectra. The core spectra (grey lines) are shown in the top panel in order of increasing redshift from top to bottom, with their best-fit models overplotted (blue lines). The outskirt spectra (grey lines) and fits (magenta lines) are similarly shown in the bottom panel. We normalise each spectrum by its median value between 4480 – 4520 Å and arbitrarily offset them in the y-direction for visibility. We do not show emission lines. This Figure serves to illustrate that many absorption lines are robustly detected for both the core and outskirt regions.

Результаты

Table 2. The results from our ALF α fits to the spatially resolved SUSPENSE spectra.

ID	Radius (R_e)		log(Age/Gyr)		[Fe/H]		[Mg/Fe]		[Mg/H]	
	core	outskirt	core	outskirt	core	outskirt	core	outskirt	core	outskirt
130040	0.25	0.58	$0.50^{+0.19}_{-0.22}$	$0.43^{+0.22}_{-0.17}$	$-0.35^{+0.19}_{-0.23}$	$-0.41^{+0.20}_{-0.22}$	$\begin{array}{c} -0.02^{+0.23}_{-0.17} \\ 0.21^{+0.12}_{-0.13} \end{array}$	$0.33^{+0.20}_{-0.22} \\ 0.33^{+0.15}_{-0.19}$	$\begin{array}{c} -0.37^{+0.23}_{-0.22} \\ 0.13^{+0.16}_{-0.23} \end{array}$	$-0.09^{+0.23}_{-0.27}$
127345	0.45	1.09	$0.50_{-0.22}$ $0.54_{-0.19}^{+0.15}$	$0.35^{+0.10}_{-0.08}$	$-0.35_{-0.23}^{+0.13}$ $-0.08_{-0.17}^{+0.14}$	$-0.07^{+0.12}_{-0.22}$	$0.21^{+0.12}_{-0.13}$	$0.33^{+0.15}_{-0.19}$	$0.13^{+0.16}_{-0.23}$	$0.25^{+0.15}_{-0.32}$
127154	0.74	1.66	$0.54_{-0.19} \ 0.66_{-0.17}^{+0.12}$	$0.13^{+0.11}_{-0.09}$	$-0.06^{+0.09}_{-0.09}$	$0.14^{+0.15}_{-0.27}$		-	-	-
127108	0.59	1.12	$0.66_{-0.17}^{+0.17}$ $0.58_{-0.13}^{+0.07}$ $0.24_{-0.05}^{+0.08}$ $0.14_{-0.04}^{+0.09}$	$\begin{array}{c} 0.43^{+0.22}_{-0.17} \\ 0.35^{+0.10}_{-0.08} \\ 0.13^{+0.11}_{-0.09} \\ 0.52^{+0.15}_{-0.14} \end{array}$	$-0.08_{-0.17}^{+0.17}$ $-0.06_{-0.09}^{+0.09}$ $-0.55_{-0.15}^{+0.14}$	$\begin{array}{c} -0.41^{+0.20}_{-0.22} \\ -0.07^{+0.12}_{-0.27} \\ 0.14^{+0.15}_{-0.27} \\ -0.39^{+0.18}_{-0.22} \\ -0.25^{+0.17}_{-0.23} \end{array}$	$0.26^{+0.20}_{-0.20}$	$0.59^{+0.17}_{-0.23}$	$-0.29^{+0.19}_{-0.20}$	$0.20^{+0.16}_{-0.26} \ -0.30^{+0.30}_{-0.27}$
129149	1.5	3.21	$0.24^{+0.08}_{-0.05}$	$0.52_{-0.14}^{+0.09} \ 0.21_{-0.08}^{+0.09} \ 0.09_{-0.06}^{+0.10}$	$-0.55_{-0.15}^{+0.14}$ $-0.12_{-0.17}^{+0.12}$	$-0.25^{+0.17}_{-0.23}$	$-0.20^{+0.27}_{-0.18}$	$-0.03_{-0.26}^{+0.32}$	$-0.34^{+0.23}_{-0.18}$	$-0.30^{+0.30}_{-0.27}$
128041	1.23	1.65	$0.14^{+0.07}_{-0.04}$	0.00 ± 0.10	0.02 ± 0.10	$-0.08^{+0.14}_{-0.23}$	$\begin{array}{c} 0.26^{+0.20}_{-0.20} \\ -0.20^{+0.27}_{-0.18} \\ 0.10^{+0.16}_{-0.14} \end{array}$	$\begin{array}{c} 0.59^{+0.17}_{-0.23} \\ -0.03^{+0.32}_{-0.26} \\ 0.13^{+0.22}_{-0.21} \end{array}$	$\begin{array}{c} -0.29^{+0.19}_{-0.20} \\ -0.34^{+0.23}_{-0.18} \\ 0.06^{+0.15}_{-0.20} \end{array}$	$0.03^{+0.27}_{-0.29}$
129133	0.77	1.92	$0.14_{-0.04}$ $0.15_{-0.05}^{+0.06}$	$0.09_{-0.06}^{+0.09}$ $0.03_{-0.06}^{+0.09}$	$-0.02_{-0.16}^{+0.13}$ $-0.20_{-0.24}^{+0.11}$	$-0.16^{+0.17}_{-0.29}$	41 — 6	-	-	-
128036	0.61	1.41	$0.13_{-0.05}^{+0.05} \\ 0.09_{-0.04}^{+0.04}$	$0.03_{-0.06}^{+0.07} \\ 0.00_{-0.04}^{+0.07}$	$-0.20^{+0.24}_{-0.24}$ $-0.27^{+0.10}_{-0.22}$	$\begin{array}{c} -0.25^{+0.17} \\ -0.08^{+0.14} \\ -0.16^{+0.17} \\ -0.27^{+0.17} \\ -0.27^{+0.17} \end{array}$	$0.18^{+0.17}_{-0.17}$	$0.30^{+0.21}_{-0.25}$	$-0.09^{+0.14}_{-0.24}$	$0.03^{+0.20}_{-0.36}$

Градиенты

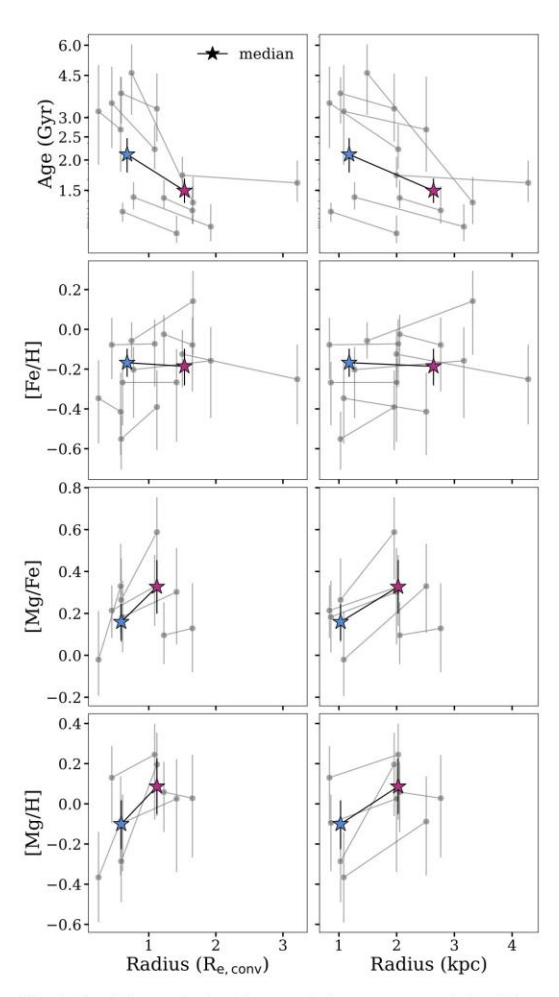


Fig. 4. Spatially-resolved stellar population parameters derived from our A = 1 full spectrum fits. In the left column, we plot our measured parameters as a function of de-projected radius in units of R_e (determined as described in Section 3.3). In the right column, we plot our measured parameters as a function of de-projected radius in units of kpc. We show age in the top row, [Fe/H] in the second row, [Mg/Fe] in the third row, and [Mg/H] in the bottom row. In each panel, we show the measured parameters for each individual galaxy as points connected by lines. We show the median parameters as stars connected by lines.

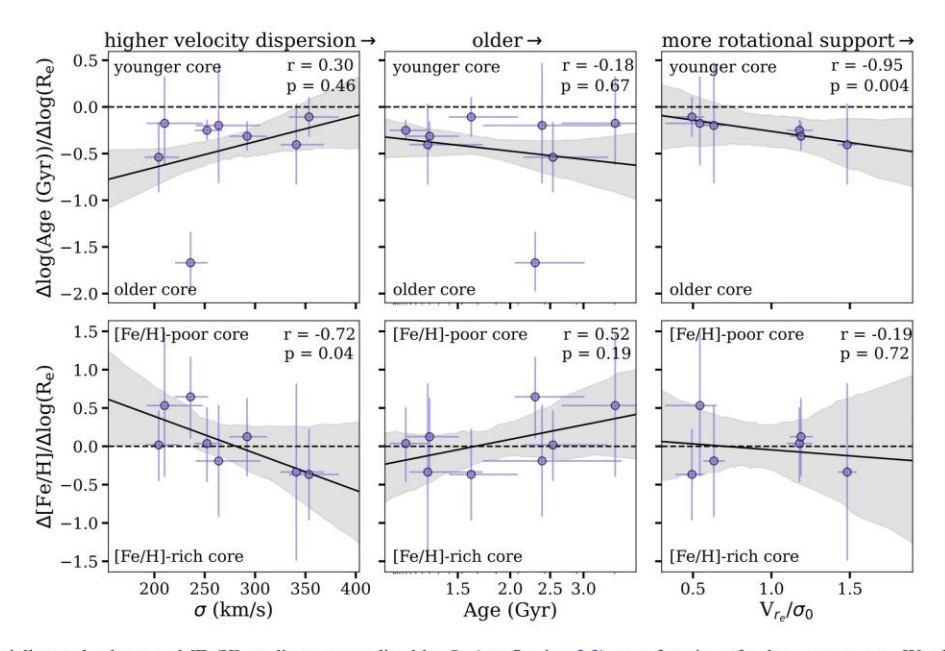


Fig. 5. Spatially resolved age and [Fe/H] gradients, normalized by R_c (see Section 3.3), as a function of galaxy parameters. We show the age gradients in the top row and the [Fe/H] gradients in the bottom row. The outlying object with a strongly negative age gradient is 127154. We show the integrated velocity dispersion (σ , from our ALF α fits to the integrated spectra) in the left column, the integrated age (from our integrated ALF α fits) in the middle, and V_{r_c}/σ_0 (measured in Slob et al. 2025) on the right. Horizontal dashed lines indicate where flat gradients would lie. We perform a linear fit to the points in each panel, shown by the solid lines, with 1σ bootstrapped uncertainties indicated by the shaded regions.

Сценарии

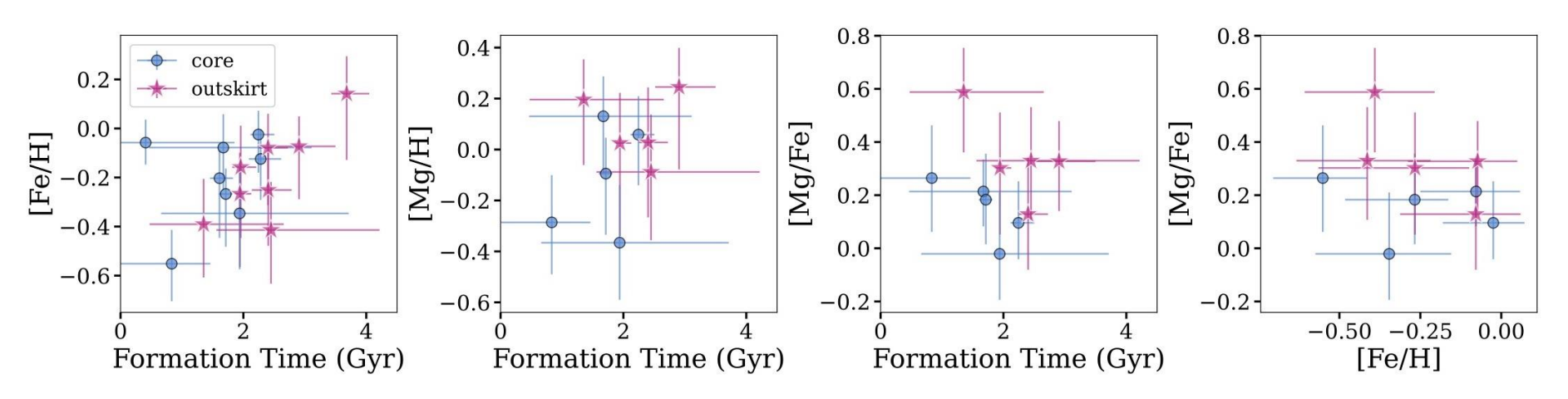


Fig. 6. Individual core and outskirt elemental abundances. In the first three panels, we show formation time on the x-axis, which we compute by correcting the stellar age (from our $ALF\alpha$ fits to the integrated spectra) by the age of the Universe at the redshift of each galaxy. We show our [Fe/H] abundances in the first panel, [Mg/H] abundances in the second panel, and [Mg/Fe] abundances in the third panel. In the fourth panel, we show [Mg/Fe] as a function of [Fe/H]. In each panel, core values are shown as points and outskirt values are shown as stars.

Выводы

• Все градиенты – НЕ ТАКИЕ, как в местных гигантских эллиптических галактиках